Multi-code Estimation of DTT Edge Transport Parameters

L. Balbinot[a], G. Rubino[b], I. Casiraghi[c,d], C. Meineri[e], L. Frassinetti[f], L. Aucone[c,d], P. Mantica[d], P. Innocente[g], M.Wigram[h], JET contributors[i], Alcator C-Mod team[h]

[a] *Università della Tuscia, Dipartimento di Economia, Ingegneria, Società e Impresa (DEIM), Via del Paradiso 47, 01100 Viterbo, Italy*
[b] *Centro Ricerche Energia, Ass. EURATOM-ENEA-CNR, CP 65 Frascati, Italy*
[c] *Dipartimento di Fisica "G. Occhialini", Università di Milano-Bicocca, Italy*
[d] *Istituto per la Scienza e Tecnologia dei Plasmi, CNR, Milano, Italy*
[e] *NEMO group, Dipartimento Energia, Politecnico di Torino, Turin, Italy*
[f] *Fusion Plasma Physics, ECSS, KTH Royal Institute of Technology, Sweden*
[g] *Consorzio RFX, Corso Stati Uniti 4, 35127 Padova, Italy*
[h] *MIT, Plasma Science and Fusion Center, Cambridge, MA 02139, USA*
[i] *See the author list of: J. Mailloux et al. "Overview of JET results for optimising ITER operation" Nucl. Fus. Special issue: Overview and Summary Papers from the 28th Fusion Energy Conference (Nice, France, 10-15 May 2021)*

Abstract

The main goal of the Divertor Tokamak Test facility (DTT) is to operate with a high value of power-exhaust-relevant parameter P_{SOL}/R in plasma scenarios similar to those foreseen for the Demonstration Fusion Power Plant (DEMO) in terms of low collisionality and neutral opacity. For these unique characteristics, accurate modelling of the principal scenario is necessary for machine designing.

In edge numerical codes, cross-field transport profiles have a high impact on modelling results. This work aims at providing a coherent set of transport parameters for DTT full-power (FP) single-null (SN) scenario edge modelling. To evaluate such parameters for DTT, a transport analysis on the current machine has been performed using SOLEDGE2D-EIRENE and SOLPS-ITER.

The transport parameters to be used in the simulations of the DTT single-

Email addresses: luca.balbinot@unitus.it (L. Balbinot), giulio.rubino@enea.it (G. Rubino), i.casiraghi3@campus.unimib.it (I. Casiraghi), carlo.meineri@igi.cnr.it (C. Meineri), lorenzof@kth.se (L. Frassinetti), l.aucone@campus.unimib.it (L. Aucone), paola.mantica@istp.cnr.it (P. Mantica), paolo.innocente@igi.cnr.it (P. Innocente), wigram@psfc.mit.edu (M.Wigram)

null scenario were selected using two complementary methods. The first is the modelling of JET and Alcator C-Mod (C-Mod) with SOLEDGE2D-EIRENE and SOLPS-ITER, validating transport parameters by comparing modelling results to experimental data from pulses which are considered *DTT-relevant*. JET pulses were selected with the highest auxiliary input power (from 29 to 33MW), plasma current and toroidal field to better match DTT parameters; nitrogen and neon seeded pulses were selected to check possible seeding material dependencies. The considered C-Mod pulse better matches DTT plasma density and neutral opacity. Transport parameters are then scaled to DTT according to scaling laws. The second method derives the transport parameters by tuning their values inside the DTT separatrix to reproduce the pedestal profiles predicted by the EPED model via the Europed code and applied in DTT.

The derived set of DTT transport parameters is consistent with the results obtained by modelling present machines, reproduces the expected heat flux decay length in detached conditions and, inside the separatrix, reproduces the predicted pedestal using transport parameters which are coherent with what is predicted by the quasi-linear turbulent model QuaLiKiz.

Keywords: `DTT`, `Soledge2D-Eirene`, `SOLPS-ITER, Divertor, Scrape-off layer`, `Edge-transport`

1. Introduction

In the framework of the European programme toward nuclear fusion [1], the role of the Divertor Test Tokamak facility (DTT) [2] [3], under construction in Frascati (Italy), will be to test alternative power exhaust solutions in an environment relevant to that of the Demonstration Fusion Power Plant (DEMO). The scope of the machine is to test physical and technological power exhaust solutions and bring them to a sufficient level of maturity to be implemented in DEMO. For this reason, the machine has been designed to operate with power-exhaust-relevant parameters like P_{SOL}/R and neutral opacity similar to DEMO.

In the designing and construction phases of new tokamaks, such as DTT, ITER and DEMO, it is necessary to predict the machine performances in the main operational scenarios. An accurate prediction of power and particle transport in the main machine scenarios is fundamental for the designing of some critical components like the divertor, the heating and pumping systems and many others. Power exhaust performances are often predicted by two-dimensional edge numerical codes such as SOLEDGE2D-EIRENE [4][5], SOLPS-ITER [6] and UEDGE [7]. These codes have no self-consistent transport treatment, transport parameters are imposed as simulation input parameters. Power exhaust performances predicted by edge modelling tools are highly dependent on particle and energy transport parameters so they must be accurately evaluated when performing predictive modelling of present and future machines.

At an initial stage, DTT edge modelling has been performed assuming uniform transport parameters [8]; now, a more sophisticated edge modelling is required for two main reasons: first, for divertor and pumping designing purposes that require accurate estimation of heat and particle deposition on the divertor targets as well as neutral distribution; second, to test the compatibility of edge requirements with core performance, H-mode compatibility and pedestal height.

This paper focuses on the definition of a validated set of transport parameters for DTT edge modelling which is a fundamental requirement for defining an accurate operational space of power exhaust-relevant parameters in DTT for designing and scenario definition purposes. Self-consistent 3-dimensional edge numerical codes such as SOLEDGE-3X [9] and EMC3 [10] would also be available in the future but were not chosen for this study because they are intrinsically slower than 2-dimensional codes. 3D modelling codes will be a precious tool for the refinement of DTT reference scenarios, for assessing turbulence and other not-axial-symmetric behaviours.

Two approaches were followed to validate a set of edge transport coefficients for DTT: the derivation of transport profiles from modelling of existing machines and the derivation from first principles modelling of DTT.

First, edge transport parameters were derived from SOLEDGE2D-EIRENE and SOLPS simulations benchmarked with experimental data from JET and Alcator C-Mod (C-Mod) pulses which can be considered compatible with the DTT single-null (SN) full-power (FP) scenario. **Section 2** describes the selection and the analysis of these pulses. This analysis led to the definition of the input parameters for SOLEDGE2D-EIRENE and SOLPS-ITER modelling of the pulses, results are described in **section 3**. **Section 4** describes the derivation of DTT edge transport parameters from first principles modelling from core modelling integrated pedestal modelling. Core modelling was performed with the JETTO suite [11], while pedestal modelling of the DTT scenario as well as performed with the Europed code [12] which implements the EPED model. In **section 5**, transport parameters derived from present machines modelling are scaled accordingly to the Eich scaling [13] and compared to those derived from DTT core and pedestal modelling. The combination of this information leads to the definition of a standard set of DTT transport parameters.

2. Pulse selection and analysis

To evaluate DTT SN transport parameters, pulses from machines which are "compatible" to DTT SN scenario were used; the main characteristics of this scenario are listed in table 2. DTT is a high-field compact machine with relatively high plasma density, current, collisionality and auxiliary input power. These features make DTT a machine with unique characteristics, and there is not a single machine which operates under *"DTT-like"* conditions. Consequently, two machines were selected for transport parameter evaluation, JET and C-Mod which are considered *DTT-revelant* for opposite reasons. Table 1 shows the main physics parameters of DTT, JET and Alcator C-Mod.

C-Mod is a high field machine which operates with relatively high core and separatrix density like DTT. The C-Mod pulse that was selected (see table 2) has a similar Greenwald fraction to DTT and a low (null) net particle flux from the core. On the other hand, JET is much more similar to DTT in terms of

parameter	DTT	JET	C-Mod
R $[m]$	2.15	2.98	0.67
a $[m]$	0.70	0.94	0.22
B_T $[T]$	6.0	3.2	2.4-8.1
I_p $[MA]$	6.0	3.5	0.24-2.0
n_e $[\times 10^{20} m^{-3}]$	1.7	0.9	0.2-8.0
T_e $[keV]$	3.1	1.7	< 9
ρ^* $[10^{-3}]$	2.9	4	2-6
β_N	1.5	1.8	< 1.8
ν^* $[10^{-2}]$	2.6	8.6	6-10

Table 1: DTT [3], JET[14] and C-Mod[15] main physics parameters.

machine dimensions, plasma current, normalized collisionality, nomalized gyro-radius and auxiliary input power. Four JET pulses were selected for the analysis, the principal characteristics of those pulses are listed in table 2; all the pulses have high auxiliary input power. The selected JET pulses have slightly higher P_{aux}/R than C-Mod, but it is lower than DTT by a factor of 2. To have a more general analysis, we selected pulses with different impurity seeding (none, nitrogen and neon, with neon being considered also a possible seeding impurity for DTT), different strike point positions and slightly different separatrix density (2.5 to $5 \times 10^{19} m^{-3}$). Two JET pulses were modelled with both SOLEDGE2D-EIRENE and SOLPS-ITER to identify possible differences between transport parameter predictions between the two codes. For geometrical reasons, only pulses with vertical-vertical strike-point positions were modelled with SOLPS.

Since the intent of this work is to derive transport parameters for steady-state inter-ELM modelling of DTT, JET and C-Mod equilibria are derived from an instant of the flat-top, the experimental data are derived from a time window of about 1 s around the selected instant.

The simulation domain of both edge codes is extended to the pedestal top ($\rho_{tor,norm} \simeq 0.9$). The input power in the simulation (P_{in}) is calculated as:

$$P_{in} = P_{aux} - P_{rad,in} - P_{ELM}, \tag{1}$$

pulse/sc. t[s]	JET 96482 51.5 ± 0.5	JET 96139 55.0 ± 0.5	JET 95946 55.0 ± 0.5	JET 92436 50.2 ± 0.5	C-Mod 1160729008	DTT S.N. -
B_T[T]	3.29	2.70	2.65	2.80	7.8	5.85
I_P[MA]	3.5	2.5	2.5	3.0	1.4	5.5
q_{cyl}	2.7	2.4	2.4	2.3	4.0	2.2
R_{ax}[m]	2.97	3.03	3.04	3.05	0.68	2.19
a[m]	0.92	0.85	0.90	0.95	0.22	0.7
$\langle n_e \rangle$ $[\times 10^{20} m^{-3}]$	2.1	2.8	2.1	1.8	4.3	1.7
f_g	0.77	0.9	0.9	0.9	0.47	0.45
Str.point	C-C	V-V	V-V	C-C	V-V	V-V
Seeding	Ne	-	N	Ne	-	Ne/Ar
P_{aux}[MW]	33.3	28.5	28.6	32.8	5.0	44.8
Γ_D^{core} $[\times 10^{20} s^{-1}]$	26.7	22.1	23.6	26.5	0.0	1.1
code	soledge	sol./solps	sol./solps	soledge	soledge	

Table 2: Main power exhaust-relevant parameters of DTT and JET and C-Mod pulses that were selected for transport parameters evaluation. *C-C* and *V-V* stand for *corner-corner* and *vertical-vertical* strike point position.

where $P_{aux} - P_{rad,in}$ is the power crossing the surface relative to the domain inner boundary obtained by subtracting the power radiated inside the simulation domain from the auxiliary input power. P_{ELM} is the power that accumulates on the pedestal during the inter-ELM phase, so it does not cross the separatrix, therefore it is subtracted in the power balance. This method was used for JET discharges, P_{ELM} was not included in C-Mod analysis.

P_{aux} is derived by summing up the contributions of each auxiliary input power. $P_{rad,in}$ is calculated by integrating inside a polygon, that corresponds to the simulation inner boundary, the two-dimensional emissivity reconstruction obtained from bolometer data, see figure 1; the uncertainty associated with this method is about 10%. In two JET cases (#92436 and #96482), the high tungsten content is responsible for the elevated low-field-side radiation, see figure 1a; in those cases, the edge code inner boundary is posed outside of the radiative volume. The other two cases have low core and higher X-point radiation as in figure 1b.

P_{ELM} is calculated as the time derivative of the diamagnetic energy during the inter-ELM phase. In JET, since during an ELM the erosion from both divertor targets rapidly increases, the BeII emission line derived from spectrometer emission lines was used as the ELM trigger signal, see figure 2. P_{ELM} is obtained by sampling over 10 inter-ELM intervals, the variance is about 10%.

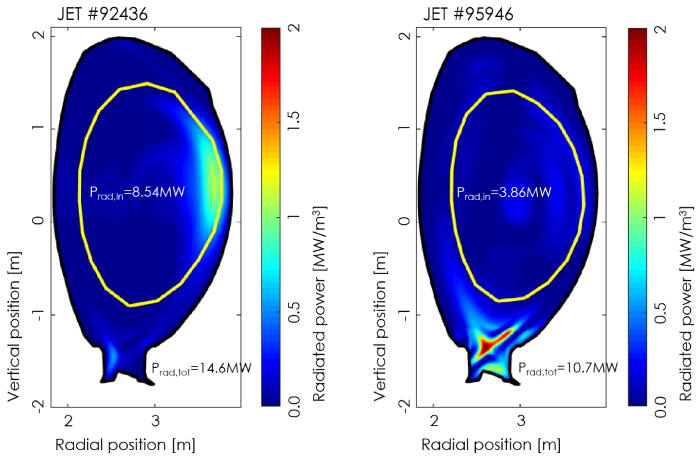

(a) JET #92436, attached neon seeded pulse with elevate tungsten content, the inner boundary is posed outside of the high radiation volume.

(b) JET #95946, nitrogen seeded discharge with lower tungsten content, lower tungsten radiation in the core and high X-point radiation.

Figure 1: Tomografic reconstruction of emissivity from bolometer data.

In the next section, the modelling of JET and C-Mod is described as well as the comparison with experimental data. Inter-ELM data from Langmuir probes, Thomson scattering and other diagnostics are excluded. The filter is applied by using the BeII signal to label the intra-ELM time, data within those time intervals are filtered out.

3. Modelling of present experiments

The modelling of the C-Mod pulse is accurately described in [16] while the JET modelling methodology is similar to that used by Rubino [17] to evaluate JT-60SA transport coefficients. The modelling is performed by fixing all the

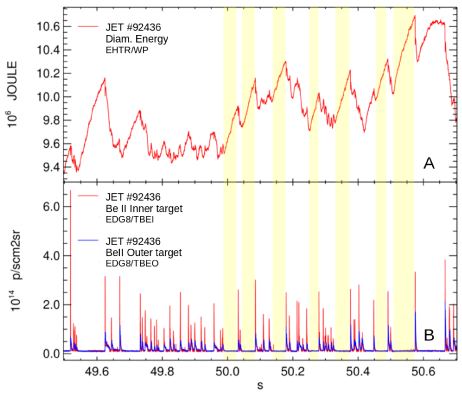

Figure 2: Time trace of the diamagnetic energy of pulse #92436, intra-ELM intervals are drown in yellow (A). BeII signal (same pulse) from the inner divertor line-of-sight of the spectrometer used to evaluate the ELM times (B).

input parameters and tuning the transport profiles to reproduce the experimental data. The upstream profiles are compared to the high-resolution Thomson scattering data, downstream profiles are compared to Langmuir probes data. For JET pulses, bolometer and spectrometer LOSs data were also available used as a further confirmation of the agreement between simulation profiles and experimental data.

Some input parameters were fixed according to the experimental some others are derived from the composition of multiple measurements like the total input power (P_{in}) described in the previous section. Thomson scattering and CXRS (charge-exchange recombination spectroscopy) show that the electron and ion temperature at the pedestal top are equal; for simplicity, we use the same cross-field heat transport profile for ions and electrons so there is only one parameter to tune. $\mathrm{P}_{in} = \mathrm{P}^e_{in} + \mathrm{P}^i_{in}$ was kept constant, the power split between the ionic and electronic channel (P^i_{in} and P^e_{in}) was set to obtain $T_i = T_e$ at the pedestal top.

Since there is no direct information on particle speed, no information could be derived on the momentum transport coefficient ν. Thus, a uniform value $\nu = 0.2\,\mathrm{m}^2/\mathrm{s}$, which is the typical value used in ITER and DEMO simulations,

was assumed over the entire simulation domain.

Fueling, impurity puffing value and their locations are taken from experimental data. In JET simulations, pumping is set to reproduce the experimental separatrix density. In all the simulations, the calculated pumping speed required to match the experimental $n_{e,sep}$ is about $180\,\mathrm{m}^3/s$ which is the typical JET pumping speed. D^+ net flux at the inner boundary is equal to the NBI particle flux. In C-Mod there is neither NBI particle flux nor fueling in the considered time interval, the total initial particle content is set and plasma density is sustained by wall recycling; more details can be found in [16]. Other input parameters like the secondary electron emission and the sheath limiter coefficients were set equal in the two codes as it was done in a recent SOLEDGE2D-SOLPS code comparison [18].

Figure 3 shows the reproducibility of C-Mod profiles with SOLEDGE2-EIRENE; the transport profiles used to reproduce experimental data are plotted in black in figures 5a and 5b. Figures 3a and 3b show a good agreement of modelling results with experimental data. Figure 3a shows that the density increases inside the pedestal $\psi_{norm} < -0.02$ even though there is no core particle flux and the neutral penetration is almost null in that region. This implies that to obtain a better reproducibility of experimental data within the pedestal top, the pinch contribution should be considered. This is beyond the scope of the work and will be investigated in future works.

An example of SOLPS and SOLEDGE2D-EIRENE modelling results for a JET pulse is shown in figures 4a-4d. Both codes could reproduce the mid-plane and target experimental data (in the figures we plot the outer target data). In C-Mod case, a pinch effect may be included to better reproduce the experimental density profile, for concistency, this was not done in this work.

The pre-ELM experimental data were fitted using a modified hiperbolic tangent function using the approach described in [19]. Figures 5a and 5b also show the similarity of the experimental profiles used in the two codes to reproduce the experimental data (continuous and dashed green lines). Results from the two edge codes are similar even if two different lists of EIRENE reactions

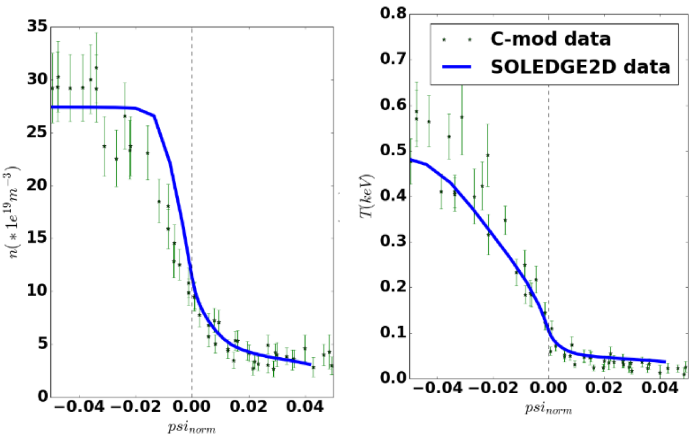

(a) C-Mod mid-plane electron density

(b) C-Mod mid-plane electron temperature

Figure 3: Midplane profiles from C-Mod modelling and experimental data.

were used, SOLEDGE2D simulations did not include D_2^+ charge exchange and neutral-neutral collisions. These reactions do not play a major role because all the considered pulses were attached.

Figure 4d shows that in JET both codes hardly reproduce the outer target temperature peak position while the peak value is correct. This may be linked to an over-estimation of the near-SOL heat transport coefficient which is required in both codes to correctly estimate the temperature peak value.

In JET cases, which have high core particle fluxes, the diffusive model could reproduce the experimental pedestal profiles and their fit at 95% of the ELM cycle, meaning that the inward pinch, if relevant, could be reproduced with a reduction of the effective D profile.

Figures 5a and 5b show some of the transport profiles derived from the modelling of JET and C-MOD. The estimations of particle transport profiles are very similar, especially the pedestal/separatrix estimations which are extremely compatible. All the estimations from different pulses or machines are in the range $D_{ped} = 0.32 \pm 0.06\,\mathrm{m}^3/\mathrm{s}$ which are compatible estimations. On the other hand, pedestal/separatrix χ estimations are spread over a wider range. This

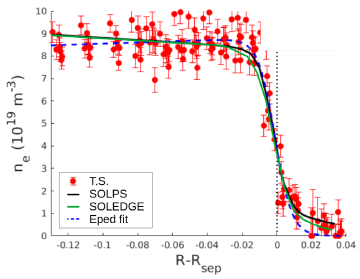

(a) JET #96139 experimental and modelling mid-plane n_e

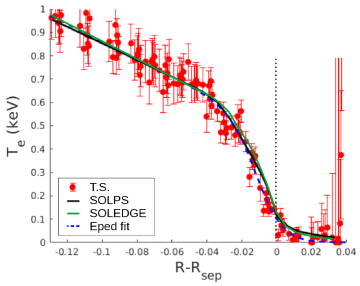

(b) JET #96139 experimental and modelling mid-plane T_e

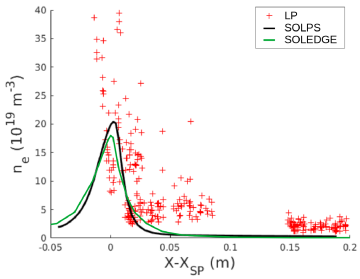

(c) JET #96139 experimental and modelling outer target n_e

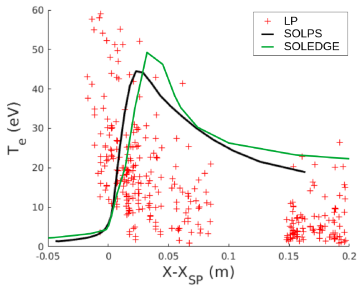

(d) JET #96139 experimental and modelling outer target T_e

Figure 4: JET #96139 at $t = 55.0 \pm 0.5$ s mid-plane and outer target experimental data (red), fit to the experimental experimental data fitted (dashed blue) and modelling profiles from SOLPS (black) and SOLEDGE2D-EIRENE (green).

was expected because the pulses have different heat flux decay lengths (λ_q), the scaling of this parameter according to the expected DTT λ_q is described in section 5.

In all the considered cases, the far-SOL transport parameters were equal and their values are $D_{f.S./Div} = 0.5\,\mathrm{m}^3/\mathrm{s}$ and $\chi_{f.S./Div} = 1.0/1.5\,\mathrm{m}^3/\mathrm{s}$.

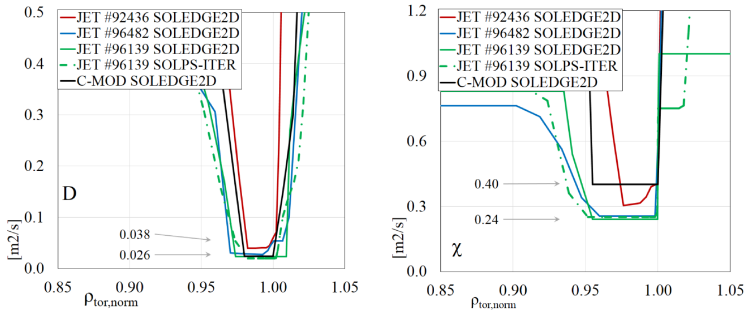

(a) Cross-field particle transport profiles "D" obtained from edge modelling.

(b) Cross-field energy transport profiles "χ" obtained from edge modelling.

Figure 5: Collection transport profiles (plotted as function of $\rho_{tor,sep}$) obtained from edge modelling of JET and C-MOD pulses.

4. DTT core and pedestal modelling

DTT edge and pedestal transport profiles can also be derived from first-principles core and pedestal modelling. In such modelling, transport parameters (as well as internal drifts) are simulation outputs consistent with the plasma profiles; the purpose was to compare these estimations of DTT transport profiles with those obtained from present machine modelling.

Core modelling of the DTT SN FP scenario has been performed with the JETTO suite [20]. This first-priciple based core modelling is extended up to the separatrix. In order to determine the FP pedestal, some specific runs of Europed code using the EPED model have been carried out. Previous DTT edge modelling activity [8] indicated that the minimum separatrix density that allows sustainable divertor conditions in the DTT FP scenario is $\langle n_e \rangle \simeq 8.0 \times 10^{19} m^{-3}$, so a pedestal with this separatrix density was generated with the Europed code.

DTT core modelling was performed with a feedback on the neutral particle influx which allowed for reproducing Europed pedestal. In the core simulations, the tubulent transport is calculated by the quasi-linear model QuaLiKiz [21], while the neoclassical transport is computed by the NCLASS [22] model. The transport coefficients include both the neoclassical and turbulent contributions. For further details see [20].

Transport profiles derived from this modelling activity are shown in the next section pictures in purple continuous and dashed lines. The transport parameters derived from core and pedestal modelling are the effective particle transport coefficient which also includes the internal pinch effect calculated as:

$$D_{eff} = D + v_P \frac{n}{\nabla n}, \tag{2}$$

where D and v_P are the transport coefficient and the pinch velocity calculated by the JETTO suite. The estimation of transport parameters from present machine modelling should be compared to D_{eff} instead of D, because pinches were not considered in the edge modelling and their effect, if relevant, is completely included in the D profiles.

It should also be pointed out that from JETTO modelling we obtain two different estimations from χ_i and χ_e since the two channels are separately self-consistently treated and the power split in the two channels is always calculated. In the next section, it will be shown that the estimation of χ_i and χ_e are similar (within a factor of 1.5) which confirms the consistency of the assumption that was made in the edge modelling of present machines.

5. Transport parameter definition

Transport profiles at the separatrix determine the cross-field decay length of density, temperature and particle flux and determine particle and power deposition distribution at the divertor targets. The Eich scaling [13] predicts a lower λ_q for DTT than for present machines like JET and C-Mod. Since the separatrix heat transport parameter determine λ_q, it is needed to re-scale to DTT the χ profiles obtained from the modelling of present machines.

With simple assumptions, the two-point model [23][24] links χ to λ_P according to the equation:

$$\chi = \frac{1}{6.4 n_e} \left(\frac{k_0^2 N^4 P_{SOL}^5}{R^9 a^5 k^{5/2} q_{95}^4} \right)^{1/7} \lambda_q^{9/7}, \tag{3}$$

$N = 1$ is the number of nulls in the poloidal field, P_{SOL} is the power crossing the separatrix, n_e is the separatrix density, R and a are the major and minor radius, k is the elongation and k_0 is the conduction coefficient of the Spitzer Harm equation:

$$k_0 = \frac{(4\pi\epsilon_0)^2}{m_e^{1/2} \ln \Lambda e^4 Z}. \tag{4}$$

By substituting in equation 3 all the parameters from present machine scenarios and the λ_q from the Eich scaling, it is possible to calculate the separatrix heat transport profile derived from the Eich scaling that will be named χ^{Eich}; the same is done for the DTT FP scenario. The scaling factor of heat transport coefficient from present machines to DTT that reflects the λ_q difference can be estimated according to equation 5, as the ratio between the χ^{Eich} estimation in DTT and present machines:

$$S_{JET/C-Mod} = \frac{\chi_{DTT}^{Eich}}{\chi_{JET/C-Mod}^{Eich}}. \tag{5}$$

Usual values of the scaling parameter are $S_{C-Mod} \simeq 0.44$ and $S_{JET} \simeq 0.34$.

One of the limits of the methodology applied is that the 2-point model and Eich scaling gives us reliable estimations in attached or high recycling regimes. All the considered pulses are in such regimes; on the other hand, DTT due to the high $\mathrm{P}_{aux}/\mathrm{R}$ fraction, will need to operate with detached divertor plasma. A broadening of λ_q to the Eich scaling is expected with detached divertor conditions and with high collisionality regimes, this phenomenon may reduce the accuracy of our predictions.

The transport parameters derived from the present machine modelling with separatrix χ scaled to DTT are plotted in figure 6. After the scaling, χ at the separatrix and pedestal are much more similar to each other with $\chi_{ped} = 0.12 \pm 0.02\,\mathrm{m}^2/\mathrm{s}$. The figure also shows DTT χ_e and χ_i profiles (purple dashed

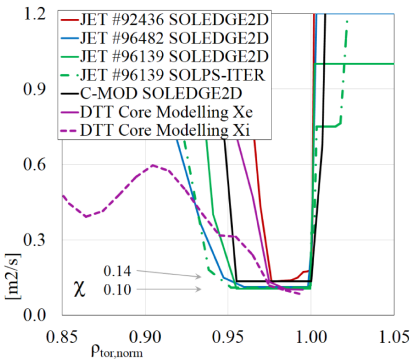

Figure 6: Transport profiles derived from present machine modelling with separatrix χ scaled to DTT. χ_e and χ_i from core modelling are plot in purple dashed and continous lines respectively.

and continuous lines respectively) obtained from DTT core modelling performed with the JETTO suite. With $\chi^{core}_{e,ped} \simeq \chi^{core}_{i,ped} \simeq 0.10\,\mathrm{m}^2/\mathrm{s}$, the estimation of both electron and ion transport profiles at the pedestal from DTT core modelling have a very good compatibility with those derived from edge modelling of present machines. The variance of the estimations of pedestal χ is about 20% of the average value which is consistent with the methodology applied and the measurement uncertainties.

A set of transport parameters was derived for DTT SN simulations by averaging the pedestal transport profiles derived with different methodologies. The transport profiles are plotted in figure 7a and 7b in black lines.

Pedestal χ and D are extended by 1 and 2 mm in the near SOL to respect the heat-flux decay length expected from the Eich scaling. D profile inside the pedestal was taken from the core modelling since in that region, the first principle-based modelling is more accurate. The D profile predicted by core modelling, differently to JET, does not increase much inside the pedestal, a similar behaviour was observed in C-Mod. It is reasonable that those two machines have a similar behaviour because DTT NBI particle flux is negligible with respect to the neutral penetration (1 order of magnitude lower) similarly to C-Mod where the flux is null; in JET instead, the density profile is almost

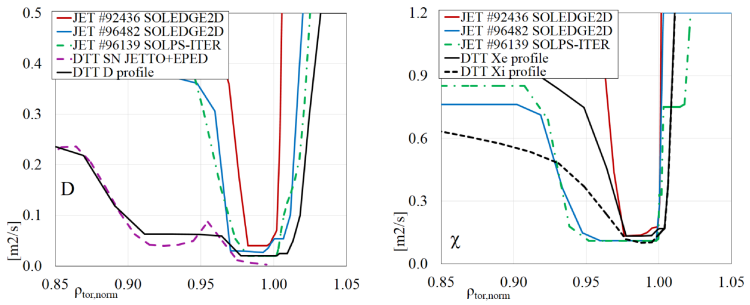

(a) D (b) χ

Figure 7: Proposed DTT SN FP transport profiles and a selection of transport parameteters derived from core and edge modelling.

equally sustained by the two fluxes.

For similar reasons, χ_i and χ_e profiles inside the pedestal are taken from core modelling. χ_i and χ_e should be differentiated if DTT edge modelling is performed using the power balance provided from core simulations to split the power flowing to the ionic and electronic channels. Transport profiles in the far-SOL and below the X-point were the same that were used in present machines edge modelling: $D_{f.S.} = 0.5\,\mathrm{m}^2/\mathrm{s}$ and $\chi_{f.S.} = 1.0\,\mathrm{m}^2/\mathrm{s}$.

6. Conclusions

A set of JET and C-Mod pulses compatible with the DTT SN scenario were selected and analysed. SOLPS and SOLEDGE2D-EIRENE modelling was performed by tuning the transport parameters to reproduce the experimental data; good reproducibility of experimental data was proven. When the same pulse was modelled with the two codes, a good agreement was found between the transport parameter estimations obtained with the two codes. A method based on the Eich scaling and the 2-point model was used to scale transport parameters from the present machine to DTT. The multiple estimations of DTT transport parameters derived from present machines show high compatibility with each other. These pedestal transport profiles are also compatible with pedestal transport profile estimations from first-principles DTT core modelling. The

main limit of this method is that it attached high-recycling pulses and DTT needs to work detached. This validated set of transport parameters is currently being used for DTT divertor designing [25] and scenario development.

Acknowledgments

This work was performed within the 3nd cycle of MARCONI-FUSION HPC. The required computational resources were allocated under the project EM-CAD.

This work is carried out in the frame of the DTT de- sign activity. The authors are very grateful to all the colleagues involved in the DTT project for their precious contribution.

This work has been carried out within the framework of the EUROfusion Consortium, funded by the European Union via the Euratom Research and Training Programme (Grant Agreement No 101052200 - EUROfusion). Views and opinions expressed are however those of the author(s) only and do not necessarily reflect those of the European Union or the European Commission. Neither the European Union nor the European Commission can be held responsible for them.

Alcator C-Mod data were originated under DOE Award DE-SC0014264

References

[1] European Research Roadmap to the Realisation of Fusion Energy, Tech. rep.

[2] R. Martone, al. eds., DTT Divertor Tokamak Test facility Interim Design Report: A milestone along the roadmap to the realisation of fusion energy ("Green Book"), 2019.
URL https://www.dtt-dms.enea.it/share/s/avvglhVQT2aSkSgV9vuEtw

[3] R. Ambrosino, et al., DTT - divertor tokamak test facility: A testbed for DEMO, Fusion Engineering and Design 167 (2021).

[4] H. Bufferand, et al., Near wall plasma simulation using penalization technique with the transport code SOLEDGE2D-EIRENE, Journal of Nuclear Materials 438 (SUPPL) (2013). doi:10.1016/j.jnucmat.2013.01.090.

[5] H. Bufferand, et al., Numerical modelling for divertor design of the WEST device with a focus on plasma-wall interactions, Nuclear Fusion 55 (5) (may 2015). doi:10.1088/0029-5515/55/5/053025.

[6] S. Wiesen, et al., The new SOLPS-ITER code package, Journal of Nuclear Materials 463 (2015).

[7] T. Rognlien, et al., A fully implicit, time dependent 2-d fluid code for modeling tokamak edge plasmas, Journal of Nuclear Materials 196-198 (1992) 347–351, plasma-Surface Interactions in Controlled Fusion Devices. doi:https://doi.org/10.1016/S0022-3115(06)80058-9.

[8] L. Balbinot, et al., Development of dtt single null divertor scenario, Nuclear Materials and Energy 27 (2021) 100952. doi:https://doi.org/10.1016/j.nme.2021.100952.

[9] H. Bufferand, et al., Progress in edge plasma turbulence modelling—hierarchy of models from 2d transport application to 3d fluid simulations in realistic tokamak geometry, Nuclear Fusion 61 (11) (2021) 116052. doi:10.1088/1741-4326/ac2873.

[10] Y. Feng, et al., Recent improvements in the emc3-eirene code, Contributions to Plasma Physics 54 (06 2014). doi:10.1002/ctpp.201410092.

[11] G. Cenacchi and A. Taroni, Jetto a free boundary plasma transport code, ENEA-RT-TIB 88 (5) (1988).

[12] S. Saarelma, et al., Integrated modelling of h-mode pedestal and confinement in JET-ILW, Plasma Physics and Controlled Fusion 60 (1) (2017) 014042. doi:10.1088/1361-6587/aa8d45.

[13] T. Eich, et al., Scaling of the tokamak near the scrape-off layer H-mode power width and implications for ITER, Nuclear Fusion 53 (9) (sep 2013). doi:10.1088/0029-5515/53/9/093031.

[14] A. R., et al., Dtt: a divertor tokamak test facility for the study of the power exhaust issues in view of demo, Nuclear Fusion 57 (1) (2016) 016010. doi:10.1088/0029-5515/57/1/016010.
URL https://dx.doi.org/10.1088/0029-5515/57/1/016010

[15] M. Greenwald, et al., 20 years of research on the alcator c-mod tokamak, Physics of Plasmas 21 (11) (2014) 110501. arXiv:https://doi.org/10.1063/1.4901920, doi:10.1063/1.4901920.
URL https://doi.org/10.1063/1.4901920

[16] C. Meineri, al., Preliminary assessment of neon impact on dtt power exhaust with alcator c-mod transport coefficients, Offshore Mediterranean Conference (2021) OMC–2021–191.

[17] G. Rubino, et al., Assessment of scrape-off layer and divertor plasma conditions in jt-60sa with tungsten wall and nitrogen injection, Nuclear Materials and Energy 26 (2021) 100895. doi:https://doi.org/10.1016/j.nme.2020.100895.

[18] M. Moscheni, et al., Cross-code comparison of the edge codes SOLPS-ITER, SOLEDGE2d and UEDGE in modelling a low-power scenario in the DTT, Nuclear Fusion 62 (5) (2022) 056009. doi:10.1088/1741-4326/ac42c4.

[19] L. Frassinetti, et al., Spatial resolution of the jet thomson scattering system, Review of Scientific Instruments 83 (1) (2012) 013506. doi:10.1063/1.3673467.

[20] I. Casiraghi, et al., First principle-based multi-channel integrated modelling in support of the design of the divertor tokamak test facility, Nuclear Fusion 61 (2021).

[21] C. Bourdelle et al., Core turbulent transport in tokamak plasmas: bridging theory and experiment with QuaLiKiz, Plasma Physics and Controlled Fusion 58 (1) (2015) 014036. doi:10.1088/0741-3335/58/1/014036.

[22] W. A. Houlberg et al., Bootstrap current and neoclassical transport in tokamaks of arbitrary collisionality and aspect ratio, Physics of Plasmas 4 (9) (1997) 3230–3242. doi:10.1063/1.872465.

[23] C.S. Pitcher and P.C. Stangeby, Experimental divertor physics, Plasma Physics and Controlled Fusion 39 (6) (1997) 779–930. doi:10.1088/0741-3335/39/6/001.

[24] P. Stangeby, The Plasma Boundary of Magnetic Fusion Devices, 2000. doi:10.1201/9781420033328.

[25] P. Innocente, et al., Design of a multi-configurations divertor for the dtt facility, Presented in this conference (24th PSI 2022), paper presented (2022).